ANS MC2015 - Joint International Conference Mathematics and Computation (M&C), Super Computing in Nuclear Applications (SNA) and the Monte Carlo (MC) Method • Nashville, TN • April 19-23, 2015, on CD-ROM, American Nuclear Society, LaGrange Park, IL (2015)

A HIGH-ORDER LOW-ORDER ALGORITHM WITH EXPONENTIALLY-CONVERGENT MONTE CARLO FOR THERMAL RADIATIVE TRANSFER

S.R. Bolding and J.E. Morel
Department of Nuclear Engineering
Texas A&M University
College Station, TX 77843
sbolding@tamu.edu; morel@tamu.edu

CCS-2 people???
Department of Nuclear Engineering
Name of University
Address
C@name.univ.edu

ABSTRACT

We have implemented a new high-order low-order (HOLO) algorithm for solving thermal radiative transfer (TRT) problems. The low-order (LO) system is based on spatial and angular moments of the transport equation and a linear discontinuous finite-element spatial representation, producing equations similar to the standard S_2 equations. The LO solver is fully implicit in time and efficiently resolves the non-linear temperature dependence at each time step. The HO solver utilizes exponentially-convergent Monte Carlo (ECMC) to give a globally accurate solution for the angular intensity to a fixed-source, pure absorber transport problem. This global solution is used to compute consistency terms that require the HO and LO solutions to converge to the same solution. The use of ECMC allows for efficient reduction of statistical noise in the MC solution, eliminating inaccuracies introduced through the LO consistency terms. We compare results with an implicit Monte Carlo (IMC) code for one-dimensional gray test problems and demonstrate the efficiency of ECMC over SMC in this algorithm.

Key Words: List of at most five key words

1. INTRODUCTION

We have implemented a high-order low-order (HOLO) algorithm for the case of gray, one spatial dimension TRT problems. The governing equations are the radiation and material energy balance equations, i.e.,

$$\frac{1}{c}\frac{\partial I}{\partial t} + \mu\frac{\partial I}{\partial x} + \sigma_t I = \frac{\sigma_s}{2}\phi + \frac{1}{2}\sigma_a acT^4 \tag{1}$$

$$\rho c_v \frac{\partial T}{\partial t} = \int_{-1}^{1} \sigma_a I(x,\mu)\mathrm{d}\mu - \sigma_a ac(T^4), \tag{2}$$

In the above equations x is the position, t is the time, μ is the x-direction cosine of the angular intensity $I(x,\mu,t)$, and a, c, ρ, and c_v are the radiation constant, speed of light, mass density, and specific heat; σ_a, σ_s, and σ_t are the absorption, scattering, and total opacities (cm^{-1}), respectively. The desired fundamental unknowns are the material temperature $T(x,t)$ and the scalar radiation intensity $\phi(x,t) = \int_{-1}^{1} I(x,\mu,t)\mathrm{d}\mu$. The equations are strongly coupled through the gray Planckian emission source $\sigma_a acT^4$, which is a nonlinear function of temperature, and the absorption term $\sigma_a\phi$. In general, the material properties are a function of T, introducing additional non-linearity. The non-linear material properties and absorption-reemission physics lead to systems that require solution in a mix of streaming and optically-thick, diffusive regions.

Monte Carlo (MC) solution to the TRT equations is typically achieved by the implicit Monte Carlo (IMC) method, first introduced by Fleck and Cummings [1]. This method linearizes the emission source in time to eliminate the material energy equation from the system. The remaining transport equation contains an approximate emission source, as well as an effective scattering cross section representing absorption and reemission over a time step. In optically thick regions, or for large time steps, the effective scattering dominates interactions. In these diffusive regions IMC becomes computationally expensive. Additionally, the approximate linearization of the emission source is not iterated on within a time step, limiting the time step size to produce physically accurate results.

Moment-based hybrid Monte Carlo (MC) methods provide an alternative solution method. Recent work has focused on fixed-point iteration high-order low-order (HOLO) approaches [2–5]. Such methods utilize a low-order (LO) operator based on angular moments of the transport equation, formulated over a coarse spatial mesh. Physics operators that are time consuming for MC to resolve, e.g., absorption-reemission and scattering events, are moved to the LO system. Newton methods allow for non-linearities in the LO equations to be fully resolved efficiently [2]. The high-order (HO) system is defined by Eq. (1), with sources estimated from the LO solution. The HO system is solved via MC to produce a high-fidelity solution for the angular intensity. The MC estimate of the angular intensity is used to estimate consistency terms, present in the LO equations, that require the LO system to preserve the angular accuracy of the MC solution; the HO system does not directly estimate a new material temperature, eliminating stability issues that require linearization of the emission source. However, sufficient MC histories must be performed to eliminate statistical noise in the conistency terms, which can contaminate the LO solution.

In this work, we demonstrate the utility of an S_2-like LO operator in conjunction with an exponentially-convergent Monte Carlo (ECMC) method [6] for the HO solver. The ECMC algorithm allows for statistical noise to be reduced to the same order as the HOLO iteration error with significantly less particle histories than standard MC simulations. We have derived the LO operator directly from the transport equation, using a linear-discontinuous (LD) finite-element (FE) spatial discretization, such that the HO and LO solutions are consistent upon convergence. Herein we describe the algorithm and present results for two test problems.

2. The Low-Order System

For simplicity, our HOLO method will use a backward Euler discretization in time, as well as constant specific heats and cell-wise constant opacities. The time discretized equations are

$$\mu\frac{\partial I^{n+1}}{\partial x}+\left(\sigma_t+\frac{1}{c\Delta t}\right)I^{n+1}=\frac{\sigma_s}{2}\phi^{n+1}+\frac{1}{2}\left(\sigma_a acT^4\right)^{n+1}+\frac{I^n}{c\Delta t} \tag{3}$$

$$\rho c_v\frac{T^{n+1}-T^n}{\Delta t}=\sigma_a\phi^{n+1}-\sigma_a ac(T^4)^{n+1}. \tag{4}$$

where Δt is the time step size and the superscript n is used to denote the n-th time step.

In the HOLO context, the LO solver models the physical scattering and resolves the material energy spatial distribution. The LO equations are formed from angular integrals and spatial moments of Eq. (4) and Eq. (3), formed over a finite element mesh. The LO equations are similar to those used in the hybrid-S_2 method in [7], with element-wise intensity-averaged angular consistency parameters that are analogous to a variable Eddington factor. The spatial moments are taken over each spatial cell i: $x\in[x_{i-1/2},x_{i+1/2}]$, weighted with the standard linear Lagrange interpolatory basis functions. For example, the L moment operator is defined by

$$\langle\cdot\rangle_{L,i}=\frac{2}{h_i}\int_{x_{i-1/2}}^{x_{i+1/2}}b_L(x)(\cdot)\mathrm{d}x, \tag{5}$$

where $h_i = x_{i+1/2} - x_{i-1/2}$ is the width of the spatial element and $b_L(x) = (x_{i+1/2} - x)/h_i$ is the FE basis function corresponding to position $x_{i-1/2}$. The right moment $\langle\cdot\rangle_R$ is defined with weight function $b_R(x) = (x - x_{i-1/2})/h_i$. The positive and negative half-range integrals of the angular flux are defined as $\phi^+(x) = \int_0^1 I(x,\mu)\mathrm{d}\mu$ and $\phi^-(x) = \int_{-1}^0 I(x,\mu)\mathrm{d}\mu$, respectively. Thus, in terms of half-range quantities, $\phi(x) = \phi^-(x) + \phi^+(x)$. Here, it is noted that $\phi_{L,i}$ and $\phi_{R,i}$ represent the values of the scalar intensity at $x_{i-1/2}$ and $x_{i+1/2}$ that preserve the zeroth and first moments over the cell, not to be confused with $\langle\phi\rangle_L$ and $\langle\phi\rangle_R$, which represent spatial moments.

Pairwise application of the L and R basis moments with the $+$ and $-$ half-range integrals to Eq. (3) ultimately yields four radiation balance equations per cell. The streaming terms aree multiplied by factors of unity to form intensity and basis-weighted averages of μ. For example, the equation resultion from application of the L moment and positive half-range integral is

$$-2\mu_{i-1/2}^{n+1,+}\phi_{i-1/2}^{n+1,+} + \langle\mu\rangle_{L,i}^{n+1,+}\langle\phi\rangle_{L,i}^{n+1,+} + \langle\mu\rangle_{R,i}^{n+1,+}\langle\phi\rangle_{R,i}^{n+1,+} + \left(\sigma_t^{n+1} + \frac{1}{c\Delta t}\right)h_i\langle\phi\rangle_{L,i}^{n+1,+} - \frac{\sigma_s h_i}{2}\left(\langle\phi\rangle_{L,i}^{n+1,+} + \langle\phi\rangle_{L,i}^{n+1,-}\right) = \frac{h_i}{2}\langle\sigma_a^{n+1}acT^{n+1,4}\rangle_{L,i} + \frac{h_i}{c\Delta t}\langle\phi\rangle_{L,i}^{n,+}, \quad (6)$$

where the $\phi_{i-1/2}^+$ and $\mu_{i-1/2}^+$ terms represent angular averaged quantities on the face at $x_{i-1/2}$. The negative direction and R moment equations are derived analogously. Opacities are assumed constant over each element, evaluated at the average temperature in the element, i.e., $\sigma_a = \sigma_a([T_{L,i} + T_{R,i}]/2), \quad x \in (x_{i-1/2}, x_{i+1/2})$. The angular consistency terms are defined in terms of half-range averages, e.g.,

$$\langle\mu\rangle_{L,i}^+ = \frac{\frac{2}{h_i}\int_0^1\int_{x_{i-1/2}}^{x_{i+1/2}}\mu\, b_L(x)I^{n+1}(x,\mu)\mathrm{d}x\mathrm{d}\mu}{\frac{2}{h_i}\int_0^1\int_{x_{i-1/2}}^{x_{i+1/2}} b_L(x)I^{n+1}(x,\mu)\mathrm{d}x\mathrm{d}\mu}. \quad (7)$$

2.1. Material Balance Equations

To derive the LO material energy equations, first $T(x)$ is represented spatially in the LD trial space, i.e., $T(x) \simeq T_{L,i}b_L(x) + T_{R,i}b_R(x), \quad x \in (x_{i-1/2}, x_{i+1/2})$. Similarly, the emission term is represented in the material and radiation equations with the LDFE interpolant, i.e.,

$$\sigma_a acT^4(x) = \sigma_a ac\left(T_{L,i}^4 b_L(x) + T_{R,i}^4 b_R(x)\right). \quad (8)$$

The L and R spatial moments are taken of the material energy equation, using the LDFE definition for $T(x)$ and $\sigma_a acT^4(x)$. For example, the final LO material energy equation resulting from application of the L moment is

$$\frac{\rho c_v}{\Delta t}\left[\left(\frac{2}{3}T_{L,i} + \frac{1}{3}T_{R,i}\right)^{n+1} - \left(\frac{2}{3}T_{L,i} + \frac{1}{3}T_{R,i}\right)^n\right] + \sigma_a^{n+1}\left(\langle\phi\rangle_{L,i}^+ + \langle\phi\rangle_{R,i}^-\right)^{n+1} = \sigma_a^{n+1}ac\left(\frac{2}{3}T_{L,i}^4 + \frac{1}{3}T_{R,i}^4\right)^{n+1}. \quad (9)$$

2.2. Closing the LO Equations

The six degrees of freedom (DOF) over each cell i are the four moments $\langle\phi\rangle_{L,i}^+$, $\langle\phi\rangle_{R,i}^+$, $\langle\phi\rangle_{L,i}^-$, and $\langle\phi\rangle_{R,i}^-$ and the two spatial LDFE edge values $T_{L,i}$ and $T_{R,i}$. The four radiation and two material energy equations

define a system of equations for the six DOF. However, the consistency parameters (e.g., Eq. (7)) are not known a priori, and there is no relation between the volume and face averaged quantities. A lagged estimate of I^{n+1} from the previous HO solve is used to estimate the angular consistency parameters. In the HOLO context, the equations for LO unknowns at iteration $k+1$ use consistency parameters computed using Eq. (7) with the latest HO solution $\tilde{I}^{n+1,k+1/2}$ as an approximation for $I^{n+1}(x,\mu)$. For the initial LO solve, all average μ parameters are set to $\pm 1/\sqrt{3}$, yielding a solution equivalent to an S_2 solution. For this initial S_2 solve, it is necessary to renormalize radiation boundary conditions to get an accurate solution, which is standard in S_N methods. To close the LO system spatially, the usual LD upwinding approximation is used. For example, for positive flow (e.g., Eq. (6)) the face terms $\mu_{i-1/2}$ and $\phi_{i-1/2}$ are upwinded from the previous cell $i-1$ or from a boundary condition; the terms at $x_{i+1/2}$ are linearly extrapolated, computed using the L and R basis moments, e.g., $\phi^+_{i+1/2} = 2\langle\phi\rangle^+_R - \langle\phi\rangle^+_L$. Because the HO ECMC solver uses an LD representation, this LO spatial closure is inherently consistent. Because there are no spatial temperature derivatives, there is no evaluation of T at faces and thus no need for an additional closure in T.

The LD closure is not strictly positive. In particular, for optically thick cells with a steep temperature gradient, the solution is driven negative. In thick regions of TRT problems, reasonably fine spatial cells can still be on the order of millions of mean free paths; negativities with a LD representation are simply unavoidable in these cells and mesh refinement is of minimal use. Typically, for a standard LDFE method, the equations are lumped to produce a strictly positive solution. However, standard FE lumping procedures would introduce difficulties in computing the consistency terms from the HO solution. An alternative discontinuous spatial discretization is used that uses a relation between the spatial moments and outflow that produces the same result as the standard FE lumping procedure. The L and R moments are defined the same as before, preserving the same average with in a cell, but the relation between the moments and the outflow is modified to force a strictly positive outflow. For example, for positive μ, the outflow is now defined as $\phi^+_{i+1/2} = \langle\phi\rangle^+_R$. Because the basis function $b_R(x)$ is strictly positive, the outflow is inherently positive. This spatial discretization is second order in h, as compared to the third order of standard LD. This closure is only used in cells in which negativities occur.

These consistency parameters are lagged in each LO solve, estimated from the previous HO solve. For the initial LO solve, parameters are used that are equivalent to an S_2 solution for isotropic sources. If the angular consistency parameters were estimated exactly, then the LO equations are exact with respect to the chosen spatial discretization. The LO system conserves energy. The HO solver is not required to conserve energy.

2.3. Solving the Non-Linear LO System

We have used Newton's method to solve the global system of coupled LO equations, based on a typical linearization of the Planckian source with opacities evaluated at lagged temperatures, as described in [8]. Application of the first order Taylor expansion in time of the gray emission source, about some temperature T^* at some time near t^{n+1} gives

$$\sigma_a^* acT^{4,n+1} \simeq \sigma_a^* ac\left[T^{*4} + (T^{n+1} - T^*)4T^{*3}\right] \tag{10}$$

where the superscript $*$ denotes evaluation at T^*. A spatially discretized form of this expression is substituted into the emission term in the discretized material energy equations, e.g., Eq. (9). This allows for the material energy equation to be eliminated from the system, introducing effective scattering and emission sources into the right hand side of the LO radiation equations. This defines four linear equations for the four remaining radiation unknowns. Once these linear equations have been solved for ϕ^{n+1}, a new estimate of T^{n+1} can be determined using the same linearization (Eq. (10)) to conserve the total energy. This estimate of T^{n+1} can now be used as T^* to form a more accurate linearization of the emission source.

This process is repeated until $\phi^{n+1}(x)$ and $T^{n+1}(x)$ converge. The lumping-equivalent discretization discussed in the previous section is used for cells where the solution for ϕ^{n+1} becomes negative. When negativities are detected, the lumping-equivalent discretization is used within those cells and that Newton step repeated.

3. The ECMC High Order Solver

The solution to the LO system is used to construct a spatially LD representation of the scattering and emission sources on the right hand side of Eq. (3). This defines a fixed-source, pure absorber transport problem for the HO operator. This transport problem, which we refer to as the HO problem, defines a characteristic method that uses MC to invert the continuous streaming plus removal operator with an LD representation of sources. We will solve the HO problem using ECMC with adaptive mesh refinement. The ECMC algorithm allows for the statistical noise in the MC solution to be efficiently reduced to any desired precision within the limits of computational memory. Thus, the HO solve produces a globally-accurate, LD representation of the angular intensity $\tilde{I}(x,\mu)$.

The transport equation to be solved by the HO solver, with HOLO iteration indices, is

$$\mu\frac{\partial I^{n+1,k+1/2}}{\partial x}+\left(\sigma_t^k+\frac{1}{c\Delta t}\right)I^{n+1,k+1/2}=\frac{\sigma_s^k}{2}\phi^{n+1,k}+\frac{1}{2}\left(\sigma_a^k acT^4\right)^{n+1,k}+\frac{\tilde{I}^n}{c\Delta t} \tag{11}$$

where k represents the outer HOLO iteration index. Material property indices will be suppressed from now on. Here, $k+1/2$ denotes the HO solve within HOLO iteration k, whereas k and $k+1$ represent successive LO solves. The sources at k are estimated by the previous LO solve. We will solve this equation using ECMC. A more detailed description of the ECMC method can be found in [9].

In operator notation, the previous equation can be written as

$$\mathbf{L}^k I^{n+1,k+1/2}=q^k \tag{12}$$

where $I^{n+1,k+1/2}$ is the transport solution of the angular intensity based on the k-th LO estimate of q^k. The linear operator $\mathbf{L}^k$ is the streaming plus removal operator defined by the left hand side of Eq. (3).

The i-th approximate solution to Eq. (12) (i represents inner HO batches) is represented as $\tilde{I}^{n+1,(i)}$. The i-th residual is defined as $r^{(i)}=q-\mathbf{L}\tilde{I}^{n+1,(i)}$. For reference, the residual at iteration i in the HO solve is

$$r^{(i),k+1/2}=\frac{\sigma_s}{2}\phi_{LD}^{n+1,k}+\frac{1}{2}\left(\sigma_a^* aT^4\right)_{LD}^{n+1,k}+\frac{\tilde{I}^n}{c\Delta t}-\left(\mu\frac{\partial\tilde{I}^{n+1,k+1/2}}{\partial x}+\left(\sigma_t+\frac{1}{c\Delta t}\right)\tilde{I}^{n+1,k+1/2}\right)^{(i)} \tag{13}$$

where the k terms are LD in space on the coarsest mesh and are not recalculated at any point during the HO solve. The functional form of $\tilde{I}^n$ is defined over the finest space-angle mesh from the final HOLO iteration of the previous time step.

To define the ECMC algorithm, the HOLO iteration indices are dropped, as the LO estimated q^k and $\mathbf{L}^k$ remain constant over the entire HO solve. Addition of $\mathbf{L}I^{n+1}-q=0$ to the residual equation and manipulation of the result yields the error equation

$$\mathbf{L}(I^{n+1}-\tilde{I}^{n+1,(i)})=\mathbf{L}\tilde{\epsilon}^{(i)}=r^{(i)} \tag{14}$$

where I^{n+1} is the exact solution and $\tilde{\epsilon}^{(i)}$ is finite element representation of the error in $\tilde{I}^{n+1,(i)}$. The above equation is inverted yielding the Monte Carlo estimate of the error in $\tilde{I}^{n+1,(i)}$, i.e.,

$$\tilde{\epsilon}^{(i)}=\mathbf{L}^{-1}r^{(i)} \tag{15}$$

where $\mathbf{L}^{-1}$ is the Monte Carlo inversion of the streaming and removal operator. Here, we emphasize the solution $\tilde{I}^{n+1,(i)}$ represents the projection of the exact Monte Carlo solution onto the trial space. This is in general far more accurate than a standard finite element solution. For example, the LD trial space preserves the zeroth and first spatial moment over a cell; the zeroth moment is computed using a standard path-length volumetric flux tally, which is equivalent to typical volumetric averages computed in Monte Carlo calculations. The primary truncation error is in the LD representation of the right hand side source terms and residual at each iteration. Only volumetric flux tallies over all of the finest space-angle elements are used; tallies are computed for the average, slope in x, and slope in μ of $I^{n+1}(x,\mu)$ by weighting the angular flux with the appropriate basis function.

The ECMC algorithm is

1. Initialize the guess for $\tilde{I}^{n+1,(0)}$ to $\tilde{I}^{n}$ or the projection of $\tilde{I}^{n+1}$ from the latest HO solve
2. Compute $r^{(i)}$.
3. Solve $\tilde{\epsilon}^{(i)} = \mathbf{L}^{-1} r^{(i)}$
4. Compute a new estimate of the intensity $\tilde{I}^{n+1,(i+1)} = \tilde{I}^{n+1,(i)} + \tilde{\epsilon}^{(i)}$
5. Repeat steps 2 – 4 until desired convergence criteria is achieved.

The initial guess for the angular intensity $I^{n+1,(0)}$ is computed based on the previous solution for $\tilde{I}^{n}$ or from $\tilde{I}^{n+1}$ of the last batch of the previous HO solve. This estimate significantly reduces the required number of particles per time step because I does not change drastically between time steps in optically thick regions. Currently, the convergence criteria is based on $\epsilon_{rel} = \|\tilde{\epsilon}^{(i)}\|_2 / \|\tilde{I}^{n+1,(0)}\|_2$, where the norm is over space and angle.

Exponential convergence is obtained because with each inversion of $\mathbf{L}$ a better estimate of the solution is being used to compute the new residual, decreasing the magnitude of the Monte Carlo source each iteration i, relative to the solution I^{n+1}. Each Monte Carlo estimate of ϵ still has a computable statistical uncertainty. If the statistical estimate of $\tilde{\epsilon}$ is not sufficiently accurate, then the iterations would diverge. Currently, the statistical uncertainty is monitored to ensure it does not become too large relative to ϵ. Because the exact angular intensity does not in general lie within the LD trial space, the iterative estimate of the error will eventually stagnate once the error cannot be sufficiently represented by a given LDFE mesh. An adaptive $h-$refinement algorithm is used to allow the system to continue converging towards the exact solution. Once the error has stagnated, refinement is performed on some percentage of the cells based on the jump errors over each face of a space-angle cell. Each space-angle cell to be refined is divided into four equal-sized cells. The previous estimate of the angular intensity and $\tilde{I}^{n}$ are projected onto the new mesh, and the iterations continue.

3.1. Variance Reduction and Source Biasing

As in [3], because we are solving a pure absorber problem, we will allow particles to stream without absorption to reduce statistical variance in the tallies. The weight of particles is reduced deterministically along the path as they stream, with no need to sample a path length. Because particles are exponentially attenuated, the normalized weight is adjusted as $w(x) = w(x_0) exp(-|(x - x_0)/\mu|)$, where x_0 is the starting location of the path. The tallies are modified to account for the continuously changing weight. Histories are allowed to stream in this manner for 6 mean free paths before switching to analog path length sampling, preventing tracking of very small weight histories.

As another way to improve efficiency and statistics, a modified systematic sampling method [10] was used for determining source particle locations. The goal is to effectively distribute particle histories to regions of

importance, but to sample a sufficient number of histories in less probable regions to prevent large statistical noise. However, there is no need to sample histories in regions that are in equilibrium and the solution is not changing over a time step.

The residual gives a good indication of where particles are most likely to contribute to the error in optically thick cells. In the sampling algorithm the number of particle histories sampled in each space-angle cell is predetermined and proportional to the magnitude of the residual in that cell. Then for the predetermined number of histories within a cell, the source location is randomly sampled according to the source distribution within that cell. There is a relative probability cutoff such that cells with an insignificant residual will have no histories sampled there. In these regions the problem is remaining in steady state and the solution is known exactly. For cells that are significant, but have a predetermined number of histories below some preset minimum N_{min}, the number of histories sampled in that cell could be set to N_{min}. This is to limit bad statistics in low probability cells, particularly in the case of adaptively refined meshes. In this work N_{min} is set to zero for comparison purposes to keep the total number of histories constant.

3.2. Fixup Near the Wave-Front

For the HO solver, in cells near the radiation wave front, the LD trial space results in negativities in $\tilde{I}^{n+1}(x,\mu)$, as with the LO solver. Currently, we do not treat these cells specially and just check the consistency terms at the end of the HO solve and detect if they lie in the appropriate half-space. If the terms are non-physical, then they are set to S_2-equivalent terms. This may lead to artificially fast wave-speeds in certain cells. Future work will include using a different trial space in these cells that is strictly positive.

3.3. The High-Order Low-Order Algorithm

Once computed, the projected LD angular intensity $\tilde{I}(x,\mu)$ is used to evaluate the LO consistency parameters for the next LO solve. Since there is a global, functional representation of the angular intensity, LO parameters are estimated using quadrature and do not require additional tallies. The HO solver does not produce a new temperature in the thermal radiative transport (TRT) context; it is only used to estimate the angular parameters in the LO solution, which eliminates typical operator splitting stability issues that require linearization of the emission source. The solution for $T(x)$ is only estimated via the LO solution.

One HOLO fixed-point iteration denotes the process of an ECMC solve of the HO problem to estimate LO parameters, based on the current LO estimate of sources, followed by a solution of the LO system for $T^{n+1}(x)$ and $\phi^{n+1}(x)$. The HOLO iterations can be performed until the LO solutions are converged to a desired precision, within each time step. The HOLO convergence criteria is based on the convergence of the FE representation of $\phi^{n+1}(x)$ and $T^{n+1}(x)$ between successive HOLO iterations k. The consistency terms force the HO and LO solutions for $\phi^{n+1}(x)$ to be consistent to the order of the current HOLO iteration error. The HOLO algorithm, for the n-th time step, is

1. Perform a diffusion-equivalent solve of the LO system to produce $T^{n+1,0}(x)$ and $\phi^{n+1,0}(x)$
2. Solve the HO system for $\tilde{I}^{n+1,k+1/2}(x,\mu)$ using ECMC, based on the current LO estimate of the emission and scattering sources.
3. Compute LO consistency parameters with $\tilde{I}^{n+1,k+1/2}$.
4. Solve the LO system using HO consistency parameters to produce a new estimate of $\phi^{n+1,k+1}$ and $T^{n+1,k+1}$ at t_{n+1}.

5. Repeat 2 – 4 until convergence is achieved.
6. Move to the next time step.

4. Results

4.1. Marshak Wave

We will compare results of the HOLO method to IMC with a source tilting algorithm [11]. In IMC the material and radiation energy fields are discretized spatially to solve for cell-averaged values. Inaccurate spatial representation of the emission source over a cell can result in energy propagating through the domain artificially fast, yielding non-physical results referred to as "teleportation error". The IMC method uses a fixup known as source tilting to mitigate this problem. Source tilting reconstructs a more accurate linear-discontinuous representation of the emission source within a cell based on the cell-averaged material temperatures in adjacent cells. This is not necessary in our method because of the LD representation of the emission source.

For the first problem, initially the radiation and material energies are in equilibrium at 2.5E-05 keV. An isotropic incident intensity of 0.150 keV is applied at $x = 0$; the incident intensity on the right boundary is 2.5E-05 keV. The material properties are $\rho = 1$ g cm$^{-}3$ and $c_v = 0.013784$ jks/keV-g. The absorption cross section varies as $\sigma(T) = 0.001\ \rho T^{-3}$, which introduces a strong non-linearity into the problem. The simulation was ran for 5 sh (1 sh = $10^{-}8$ s) with a fixed time step size of 0.001 sh. For comparison purposes, we have not used mesh refinement, only performed one HOLO iteration per time step, and use a fixed 3 HO batches with equal number of histories per batch. A relative tolerance of 1.E-06 in the norm of $\phi(x)$ and $T(x)$ was used for the LO newton solver. Radiation energy distributions are plotted as an equivalent temperature given by $T_r = \sqrt[4]{\phi/(ac)}$. Cell-averaged quantities are plotted. Although scattering physics can be handled by the LO solver in this method [5], we have only considered pure absorber problems here.

Fig. 1a compares the cell-averaged radiation temperatures for the IMC and HOLO method with ECMC, for various number of spatial mesh cells N_c. For the HOLO solver, we have used 4 equal-sized cells in μ. The solutions agree as the mesh is converged. There is similar agreement in the cell averages due to the linear shape of the emission source over a cell. The cells at the wave front required use of the lumping-equivalent discretization during the LO solve, resulting in strictly positive solutions.

Fig. 1b compares solutions for the case of 200 cells. For the IMC solution 10^5 histories per time step were simulated; for the HOLO method only $4,000$ histories per batch (12,000 per time step) were simulated. There is significant statistical noise in the IMC solution compared to the HOLO solution. The relatively small number of histories is possible due to the residual formulation and the initial guess of $\tilde{I}^n$ for the first HO solve. Since the transport solve is only determining the change over the time step, the statistical noise in the result is small relative to the magnitude of the solution intensity. Also, the source bias only places particles where the residual is large. No particles are sampled in the equilibrium region out front of the wave.

4.2. Two Material Problem

This problem consists of an optically thin (left) and an optically thick (right) material region, with constant opacities. The material properties are given in Table I. Initially the radiation and material energies are in equilibrium at a temperature of 0.05 keV. An isotropic incident intensity of 0.500 keV is applied at $x = 0$ at $t = 0$; the isotropic incident intensity on the right boundary is 0.05 keV. The simulation is ran for 5 sh.

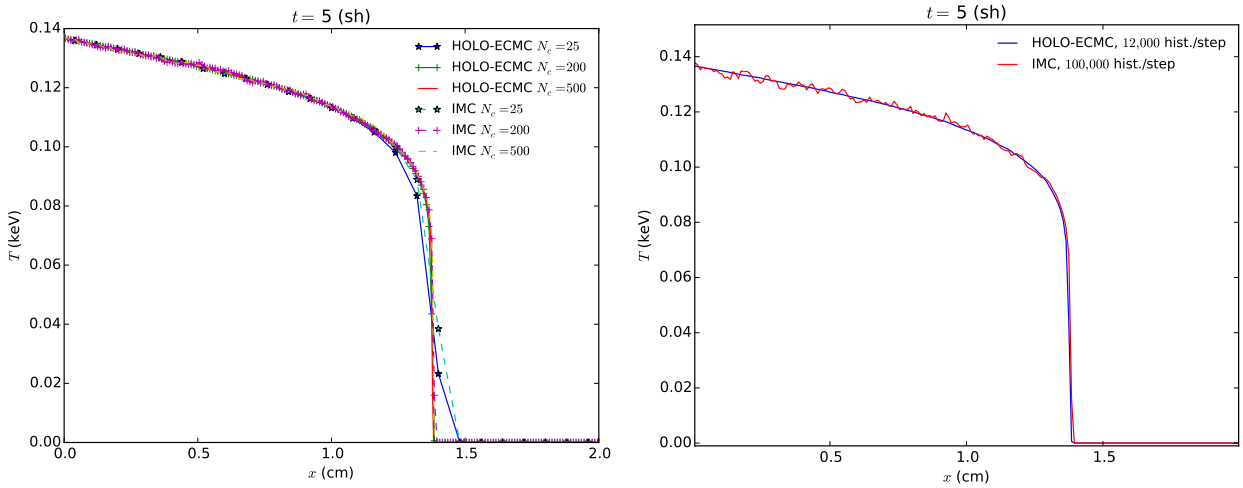

(a) Convergence of IMC and HOLO-ECMC solutions.

(b) Comparison of solutions for 200 spatial cells.

Figure 1: Comparison of solutions for Marshak wave problem at t = 5 sh.

Fig. 2b compares the HOLO and IMC radiation temperatures at the end of the simulation. The IMC method used 10^5 histories per time step, where as the HOLO method used 3×10^4 histories per time step. The IMC and HOLO results show agreement over the finer mesh. On the coarse mesh ($N_c = 25$), the HOLO method predicts the location of the wave-front more accurately than the IMC method.

Fig. **??** compares results for different HO solvers. The HOLO-ECMC results are for running 3 batches of 10,000 histories, per time step. Also plotted is the solution for the HOLO method with a standard MC solver as the HO solver (HOLO-SMC) with standard source sampling. The SMC solver uses 10^5 histories per time step. The S_2 solution uses the LO solver with diffusion-equivalent consistency terms and no MC correction. The HOLO-SMC solution demonstrates significant statistical noise. This noise is introduced into the LO solver by bad statistics in computing the consistency terms. The S_2 solution results in an artificially fast wave front, demonstrating the correction the HO solvers provide.

	$x \in [0, 0.5)$ cm	$x \in [0.5, 1.0]$ cm
σ_a (cm$^-$1)	0.2	2000
ρ (g cm$^-$3)	0.03	10.0
c_v (jks/keV-g)	0.1	0.1

Table I: Two material problem properties

5. Conclusions

We have been able to reproduce the IMC solutions for Marshak Wave test problems with a new HOLO method. Unlike IMC, our method requires no effective scattering events to be included in the MC simulation, limiting the total run time of the simulations; this is also favorable for future parallelization since particles can be allowed to stream to boundaries without interaction. The LD spatial representation mitigates issues with energy propagating through the problem artificially fast, similar in effect to source tilting in the IMC algorithm. The LO solver resolves the non-linearities in the equations resulting in a fully implicit time discretization. The ECMC approach, with initial guesses based on the previous radiation

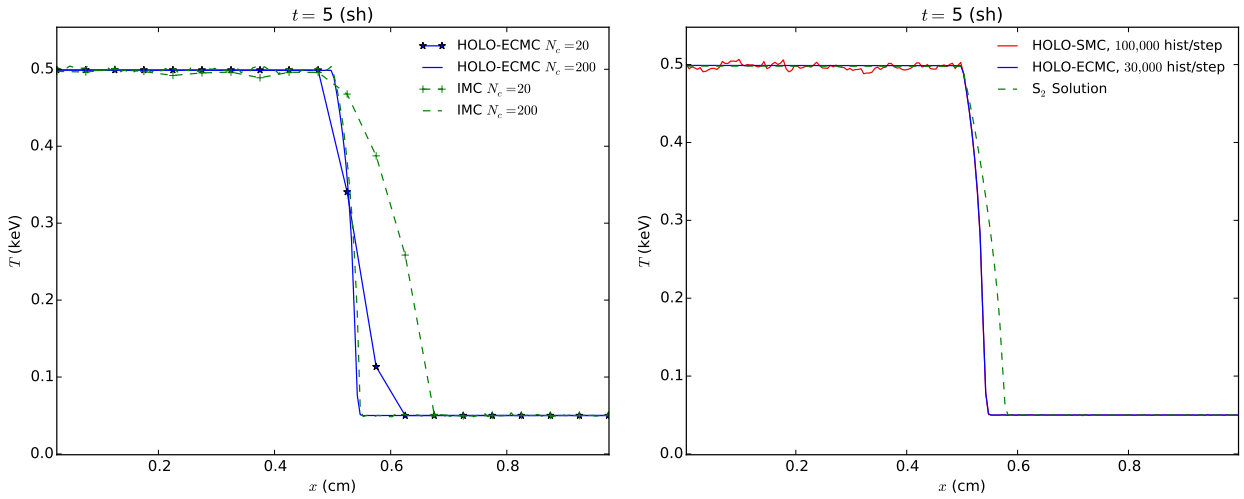

(a) Comparison of IMC and HOLO-ECMC.

(b) Comparison of SMC and ECMC HO solvers.

Figure 2: Comparison of radiation temperatures for two material problem.

intensity, results in efficient reduction of statistical error and allows for particles to be distributed to largely varying regions of the problem. The LO solver can accurately and efficiently resolve the solution in diffusive regions, while the HO transport solver provides the accuracy of a full transport treatment where necessary.

The primary difficulty to overcome is in the HO solver at the wave front. A strictly positive spatial discretization in the HO system needs to be implemented, e.g., the consistent set to zero method, for high accuracy solutions. Comparisons to semi-analytic or manufactured solutions will be performed to demonstrated the benefit of the ECMC iterations for getting high-accuracy solutions. Future work will include apllication to multi-frequency equations, before extending to multiple spatial dimensions.

ACKNOWLEDGEMENTS

This research was performed, in part, using funding received from the DOE Office of Nuclear Energy's Nuclear Energy University Programs.

REFERENCES

[1] J. A. Fleck, Jr. and J. D. Cummings, Jr., "An Implicit Monte Carlo Scheme for Calculating Time and Frequency Dependent Nonlinear Radiation Transport," *J. Comput. Phys.*, **8**, 3, pp. 313–342 (Dec. 1971).

[2] J. Willert, C. Kelly, D. Knoll, and H. Park, "A Hybrid Approach to the Neutron Transport k-Eigenvalue Problem using NDA-based Algorithms," (2013), M&C.

[3] H. Park, J. Densmore, A. Wollaber, D. Knoll, and R. Ramenzahn, "Monte Carlo Solution Methods in a Moment-Based Scale-Bridging Algorithm For Thermal Radiative Transfer Problems," M&C (2013).

[4] J. Willert and H. Park, "Residual Monte Carlo High-order Solver for Moment-Based Accelerated Thermal Radiative Transfer Equations," *Journal of Computational Physics*, **276**, pp. 405 – 421 (2014).

[5] S. Bolding and J. Morel, "A High-Order Low-Order Algorithm with Exponentially-Convergent Monte Carlo for k-Eigenvalue problems," ANS Winter Meeting (2014).

[6] J. Peterson, J. Morel, and J. Ragusa, "Exponentially Convergent Monte Carlo for the 1-D Transport Equation," M&C (2013).

[7] E. Wolters, *Hybrid Monte Carlo - Deterministic Neutron Transport Methods Using Nonlinear Functionals*, Ph.D. dissertation, Michigan (2011).

[8] J. Morel, T. Wareing, and K. Smith, "Linear-Discontinuous Spatial Differencing Scheme for S_n Radiative Transfer Calculations," *Journal of Computational Physics*, **128**, pp. 445–462 (1996).

[9] J. Peterson, *Exponentially Convergent Monte Carlo for the 1-D Transport Equation*, Master's thesis, Texas A&M (2014).

[10] J. Shultis and W. Dunn, *Exploring Monte Carlo Methods*, Academic Press, Burlington, MA 01803 (2012).

[11] T. Urbatsch and T. Evans, "Milagro Version 2 An Implicit Monte Carlo Code for Thermal Radiative Transfer: Capabilities, Development, and Usage," Los Alamos National Laboratory Report LA-14195-MS (2006).